Polarization of crack waves along an artificial subsurface fracture

Polarization of crack waves along an artificial subsurface fracture

Koji Nagano and Kazuhiko Sato

Department of Computer Science and Systems Engineering, Muroran Institute of Technology, Muroran, Japan

Hiroaki Niitsuma

Department of Geoscience and Technology, Graduate School of Tohoku University, Sendai, Japan

Abstract. We analyze three-dimensional (3D) particle motions of crack waves which propagate along a fracture to determine fracture orientation. Crack waves were measured at an artificial subsurface fracture at a depth of approximately 370 m in the Higashihachimantai Hot Dry Rock model field in Japan. Dispersion was observed in crack waves. Velocities of crack waves below 100 Hz are 100 m/s - 150 m/s along this artificial fracture. Therefore, crack waves arrived after compressional wave and shear wave. A coherence matrix is used to analyze the 3D particle motions in the frequency domain. Noise, which is outside of the band of the detector, is excluded in the coherence matrix analysis. We examine the polarization of 3D particle motions of crack waves using Principal Component Analysis. The longest axis of an ellipsoid which approximates the 3D particle motions shows a direction consistent with estimates obtained by core-sample measurements and tectonic stress measurements. The differences in fracture orientation obtained from the crack-wave analysis and the core sample analysis are less than 16° in azimuth and less than 20° in dip.

Introduction

Crack-wave measurement is a promising seismic technique for characterizing fractures because crack waves propagate along fractures and the energy of crack waves is concentrated along the fracture. Therefore, propagation characteristics of crack waves depend upon the geometry of the fracture and the elastic properties of the rock near the fracture. Many researchers have studied the dynamic motion, velocity, and distribution of displacement of crack waves in numerical fracture models [Chouet, 1986; Ferrazzini and Aki, 1987; Pyrak-Nolte and Cook, 1987; Hayashi and Sato, 1992]. Crack waves were measured in a field by authors. [Nagano et al., 1995; Nagano and Niitsuma, 1996]. Arrival of the crack waves was determined in analysis on tube waves, which crack waves generated at a borehole intersection. Because energy of crack waves is concentrated in a fluid layer of crack, crack waves which were not contaminated by compressional and shear waves could be detected by a hydrophone in this measurement. Crack waves show dispersion and their group velocities below 100 Hz are 100 m/s - 150 m/s. A symmetric mode is dominant in the crack waves.

In this paper, we describe the 3D particle motions of crack waves detected at rock layers near a subsurface fracture. We

examined the direction of this motion to estimate the orientation of the fracture.

Crack-Wave Measurements

Crack waves were detected in a field measurement at the Higashihachimantai Hot Dry Rock model field in Iwate prefecture, Japan [Niitsuma, 1989]. Figure 1 illustrates the crack-wave measurement. An artificial subsurface fracture was created in intact welded tuff at a depth of 369.0 m in well F-1 by hydraulic fracturing. During the hydraulic fracturing, 40-mesh sand was injected as a propping agent. Core samples showed no significant joint or crack before fracturing. Well EE-4 was drilled into the artificial fracture after the hydraulic fracturing, and intersected the artificial fracture at a depth of 358.2 m. The distance between the intersection points of wells F-1 and EE-4 is 6.7 m. The radius of the fracture is about 60 m [Niitsuma, 1989]. Tectonic stresses in this field were measured and the fracture orientation was estimated from the minimum compressional tectonic stress [Hayashi et al., 1989]. Azimuth and dip of minimum compressional tectonic stress are N-83.8°-E and N 50.1°, respectively. The principal stresses are not vertical and horizontal in this field. The ori-
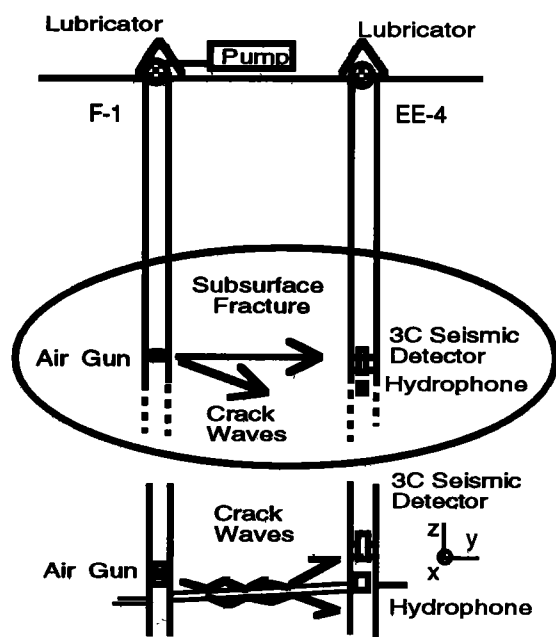

Figure 1. Field set-up for crack-wave measurements along a fracture. A core sample at the intersection of well EE-4 shows that azimuth and dip of the fracture are N-60°-E and N 47°, respectively.

entation of the fracture in a core sample, which was obtained in well EE-4, was also measured [Hayashi et al., 1989]. Azimuth and dip of the fracture in the core sample are N-60°-E and N 47°, respectively. A transmissibility test showed that the fracture aperture was about 0.08 mm without pressurization and 0.2 mm for a wellhead pressure of 3.0 MPa [Hayashi and Abé, 1989]. The velocities of compressional and shear waves of the intact rock in this field are 3000 m/s and 1750 m/s, respectively.

We measured the 3D particle motions of crack waves which propagated along this artificial fracture. A downhole air gun was used as a wave source at a depth of 367.0 m in well F-1. The air gun was suspended two meters from the intersection of the fracture so that we would not damage the borehole at the intersection. We fixed a three-component seismic detector at depths of 357.0, 357.5, and 359.0 m in well EE-4 and measured the 3D particle motions of the rock layer, which was excited by crack waves and other elastic waves. We can detect 3D particle motions in a frequency range of 150 Hz to 300 Hz using this three-component seismic detector [Nagashima et al., 1992]. The orientation of the three-component seismic detector in the borehole was measured using an onboard electric compass.

We opened the subsurface fracture with hydraulic pressure because the energy of the crack waves increases as the fracture aperture increases [Nagano et al., 1995]. The wellheads of both wells were closed with wireline lubricators. Wellhead pressure was measured in well F-1. The maximum wellhead pressure was 3.0 MPa during our measurements.

3D Particle Motions of Crack Waves

The arrival time of the crack waves was estimated as in our previous measurements on crack wave propagation [Nagano

Figure 3. 3D Lissajous patterns of the crack waves detected at a depth of 357.5 m. Data after 30 ms in Figure 2 (c) are plotted. Data length is 260 ms. Two horizontal axes, P1 and P2, are provisionally determined to show vertical Lissajous patterns. The 3D Lissajous patterns are not spherical, and a distinct direction can not be estimated.

Y: N-101.1° -E
P1: N-164.6° -E
P2: N-74.6° -E

(a) Hydrophone (358.2 m)
Crack wave arrival

(b) Vertical motion (357.0 m)

(c) Vertical motion (357.5 m)

(d) Vertical motion (359.0 m)

0 20 40 60 80
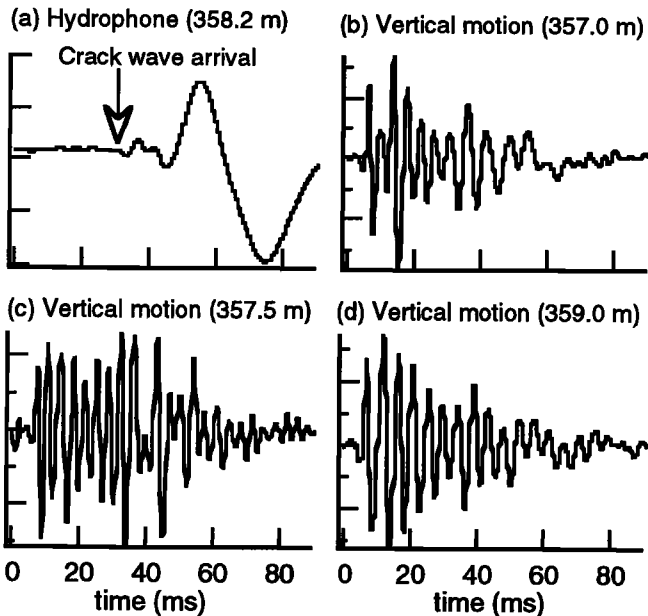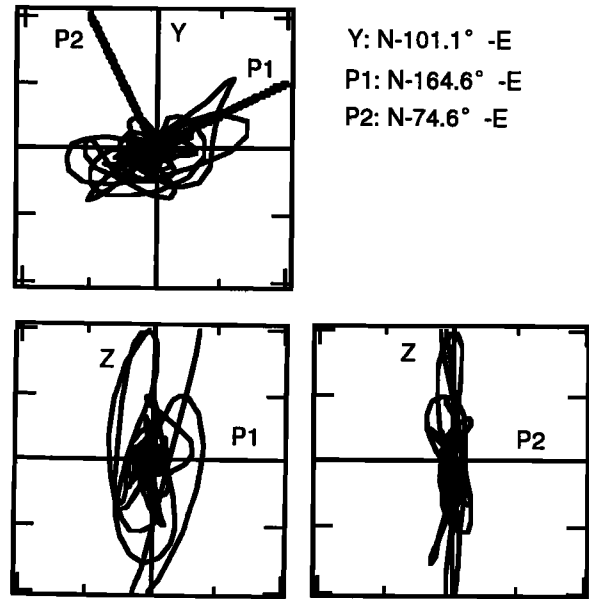time (ms)

0 20 40 60 80
time (ms)

Figure 2. Crack waves detected with a hydrophone and a 3C seismic detector at a wellhead pressure of 3.0 MPa. Vertical particle motion at depths of 357.0, 357.5, and 359.0 m are shown in Figure 2 (b)-(d). Compressional and shear waves overlap the crack waves in Figure 2 (b)-(d) after crack waves arrival, 30 ms.

et al., 1995; Nagano and Niitsuma, 1996]. In these measurements, we used a hydrophone instead of the three-component seismic detector, while the air gun was installed at the same location. The hydrophone was suspended in well EE-4 at a depth of 358.2, at the intersection with the fracture. Energy of crack waves is concentrated in a fluid layer. The hydrophone is more sensitive to fluid motion and less sensitive to rock-layer motion than the three-component seismic detector. Therefore, we can detect the arrival of crack waves with a high signal-to-noise ratio using the hydrophone. The waveform detected with the hydrophone indicates that the crack waves arrived at 30 ms.

Figure 2 shows the crack waves detected with the hydrophone and the three-component seismic detector for a wellhead pressure of 3.0 MPa. The three-component detector was fixed at three depths near the intersection. Crack waves detected with the three-component seismic detector were filtered with a FIR bandpass filter (f = 150 Hz - 300 Hz) [Oppenheim and Schafer, 1975]. Because the three-component seismic detector was fixed in the borehole, it was sensitive to compressional and shear waves in a rock layer, which arrived before the crack waves. The compressional and shear waves made it difficult to detect the arrival time of the crack waves in Figure 2 (b)-(d). However, we observed that the amplitude increased again after 30 ms in Figure 2 (b)-(d). Therefore, we concluded that the crack waves were dominant after 30 ms.

3D Lissajous patterns [Niitsuma and Saito, 1991] of the crack waves after 30 ms in Figure 2 (c) are given in Figure 3. Data length in Figure 3 is 260 ms. Since the Lissajous patterns are not spherical, the crack waves have a polarization pattern which reflects their propagation. However, it is difficult to derive a reasonable estimate of the direction of polarization based solely on Figure 3.

Coherence Matrix Analysis for Crack Waves

In Principal Component Analysis, an eigenvector for the maximum eigenvalue of a covariance matrix gives direction of an axis on which projected data have the maximum variance [Samson, 1977]. We refer to an eigenvector for the maximum eigenvalue as the first eigenvector in this paper. The first eigenvector, therefore, gives an optimum direction of an axis on which the 3D data shows the maximum energy. On the other hand, crack waves show ellipsoidal particle motion and the longest line between the foci of the ellipsoid is perpendicular to the fracture. Thus, the first eigenvector, which shows direction of the maximum energy of the 3D data, is an optimum estimate of a normal of the fracture.

We use a coherence matrix to analyze the 3D particle motions in the frequency domain [Kay, 1987]. The coherence matrix for the three-channel signal is defined as

$$A = \begin{pmatrix} 1 & \text{coh}^2_{xy}(\omega) & \text{coh}^2_{xz}(\omega) \\ \text{coh}^2_{xy}(\omega) & 1 & \text{coh}^2_{yz}(\omega) \\ \text{coh}^2_{xz}(\omega) & \text{coh}^2_{yz}(\omega) & 1 \end{pmatrix} \qquad (1)$$

where $\text{coh}^2_{ij}(\omega)$ is coherence between channels i and j. Coherence is given by

$$\text{coh}^2_{ij}(\omega) = \frac{|S_{ij}(\omega)|^2}{S_{ii}(\omega)S_{jj}(\omega)} \qquad (2)$$

where $S_{ii}(\omega)$ is the power-spectrum of channel i and $S_{ij}(\omega)$ is the cross-spectrum between channels i and j. The coherence ma-
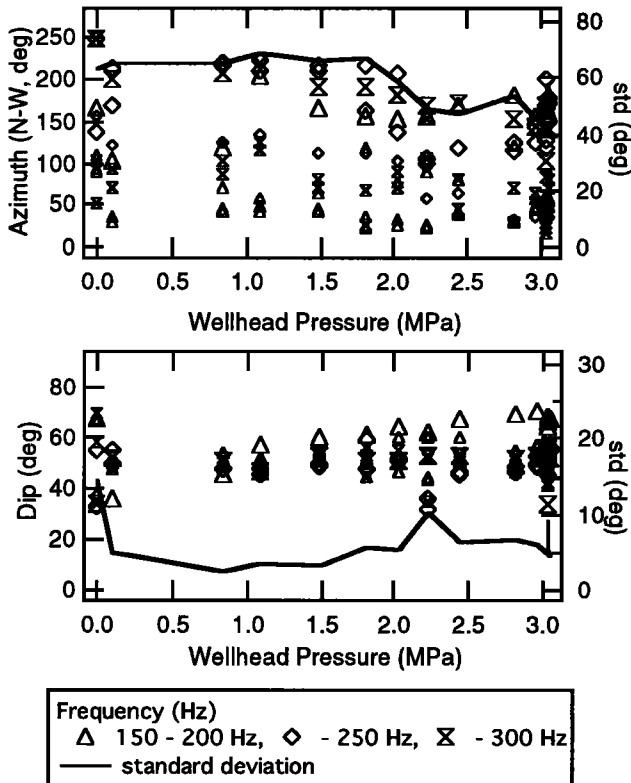

Figure 4. Azimuth and dip of the first eigenvector of the coherence matrix. The crack waves detected at a depth of 357.0 m are analyzed. Frequency components above 150 Hz are plotted.
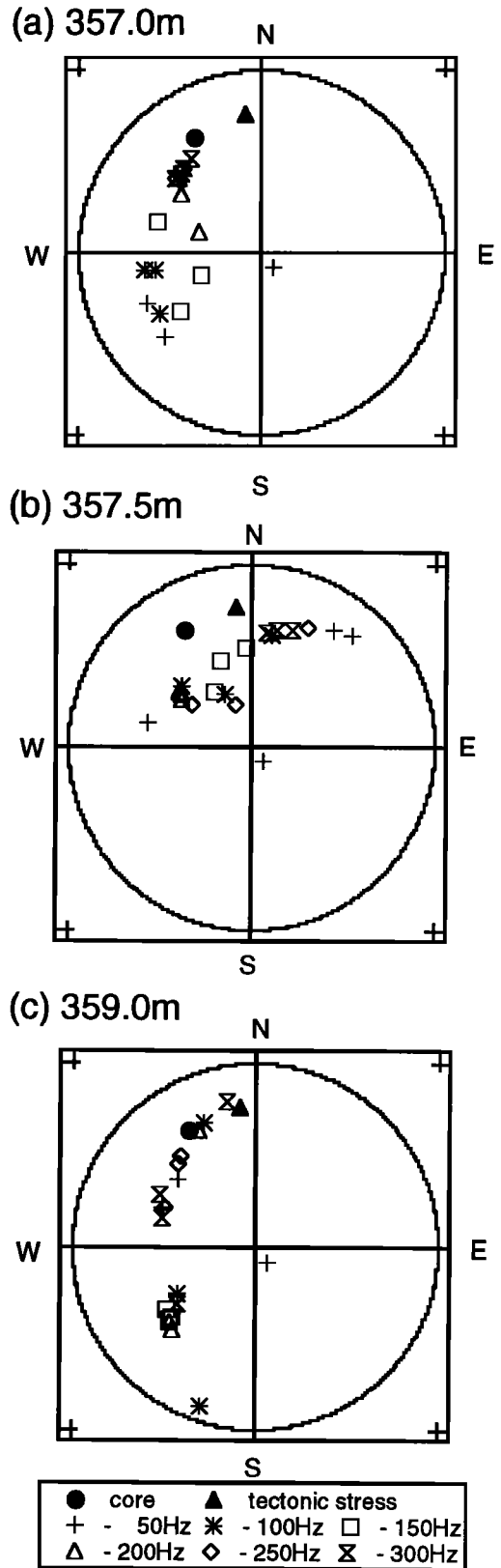

Figure 5. Directions of the first eigenvector at depths of 357.0 m, 357.5 m and 359.0 m. The crack waves were detected for a wellhead pressure of 3.0 MPa. The directions of the artificial subsurface fracture based on a core sample obtained in well EE-4 and minimum tectonic stress near the fracture are also given. The frequency components below 150 Hz are also plotted. The 3C seismic detector cannot detect precise 3D particle motions below 150 Hz.

trix represents frequency decomposition for a covariance matrix of a multidimensional signal. Therefore, the first eigenvector of the coherence matrix indicates an optimum direction of a normal of the fracture in a frequency domain. We analyze 3D waveform in a frequency domain by using coherence matrix to exclude noise and resonant frequency components.

We calculated the power-spectrum and the cross-spectrum using the Blackman-Tukey algorithm [Kay, 1987]. The duration of the data is 260 ms after the crack waves arrival. The frequency resolution in the spectral estimation is 16.6 Hz.

Figure 4 shows the azimuth and dip of the first eigenvector estimated at several wellhead pressures. In Figure 4, the crack waves detected at a depth of 370.0 m are analyzed and frequency components of 150 Hz - 300 Hz are plotted in Figure 4. Standard deviation of the estimated azimuth decreases at wellhead pressure above 1.8 MPa. When aperture of the fracture increases as a result of hydraulic pressurization, crack waves with a large amplitude can also propagate along the fracture [Ferrazzini and Aki, 1987]. Therefore, we estimated the azimuth of the first eigenvector with only small standard deviation when the wellhead pressure was increased.

The directions of the first eigenvectors, which are estimated at three locations from the waveforms detected for a wellhead pressure of 3.0 MPa, are given in Figure 5. We also plot the normal of the artificial subsurface fracture in a core sample, which was obtained from well EE-4, and the direction of minimum compressional tectonic stress, which was estimated by hydraulic fracturing at a depth of 350 m in well E-3 near well EE-4 [Hayashi et al., 1989].

The three-component seismic detector can detect 3D particle motions in a frequency range of 150 Hz to 300 Hz [Nagashima et al., 1992]. The directions of these frequency components are similar to the data obtained from the core sample and tectonic stress. On the other hand, the directions outside of this band are different than those obtained by these other measurements.

The directions estimated at a depth of 357.5 m are closest to those using the other two techniques at the three locations for the three-component detector. This agrees with the notion that the energy of the crack waves decreases in a direction normal to the fracture. The differences in fracture orientation between the crack-wave analysis and the core sample analysis are less than 16° in azimuth and less than 20° in dip.

Discussion

The fracture orientation estimated from crack waves agrees with those obtained from core samples and tectonic stress measurements. However, measurement techniques with higher signal-to-noise ratios and more sensitive three-component seismic detectors should be investigated to improve the accuracy and reliability of the crack-wave measurements.

Because crack waves are slower than bulk waves, the coda of the bulk waves might overlap with the crack waves. Such overlap can cause errors in the analysis. The separation between the wave source and sensor should be made long enough so that bulk waves do not overlap with crack waves. It is also important to increase the amplitude of the crack waves. The results of our measurement have shown that opening the frac-

ture and making observations close to the fracture are effective for decreasing dispersion of the estimated directions.

As shown in Figure 5, the directions of the frequency components outside of the bandwidth of the three-component seismic detector are different than those estimated using the other two measurements. 3D particle motions should be analyzed only in the frequency range where precise 3D particle motions can be detected. Furthermore, broad band measurement provides more data in the coherence matrix analysis. It improves reliability of spectral estimation.

References

Chouet, B., Dynamics of a fluid-driven crack in three dimensions by the finite difference method, *J. Geophys. Res., 91*, 13967-13992, 1986.

Ferrazzini, V. and K. Aki, Slow waves trapped in a fluid-filled infinite crack: implication for volcanic tremor, *J. Geophys. Res., 92*, 9215-9223, 1987.

Hayashi, K., T. Ito and H. Abé, In situ stress determination by hydraulic fracturing - A method employing an artificial notch, *Int. J. Rock Mech. Min. Sci. Geomech. Abstr., 26*, 197-202, 1989.

Hayashi, K. and H. Abé, Evaluation of hydraulic properties of the artificial subsurface system in Higashihachimantai geothermal model field, *J. Geothermal Res. Soc. Jpn, 11*, 203-215, 1989.

Hayashi, K. and K. Sato, A theoretical study of AE traveling through a fluid-filled crack with application to characterization of a geothermal reservoir crack, In T. Kishi, K. Takahashi & M. Ohtsu (eds.), *Progress in Acoustic Emission VI:* Fukuoka: The Japanese Society for NDI. 423-430, 1992.

Kay, S. M., *Modern Spectral Estimation Theory and Application*, 446 pp., Prentice Hall, Englewood Cliffs, New Jersey, 1988.

Nagano, K., H. Saito and H. Niitsuma, Guided waves trapped in an artificial subsurface fracture, *Geothermal Sci. Technol., 5*, 63-70, 1995.

Nagano, K. and H. Niitsuma, Crack stiffness from crack wave velocities, *Geophys. Res. Lett., 23*, 689-692, 1996.

Nagashima, S., H. Moriya and H. Niitsuma, Development and calibration of downhole triaxial AE detectors for subsurface and civil engineering AE measurement, In T. Kishi, K. Takahashi & M. Ohtsu (eds.), *Progress in Acoustic Emission VI:* Fukuoka: The Japanese Society for NDI. 423-430, 1992.

Niitsuma, H., Fracture mechanics design and development of HDR reservoirs -concept and results of the Γ-project, Tohoku University, Japan, *Int. J. Rock Mech. Min. Sci. Geomech. Abstr., 26*, 169-175, 1989.

Niitsuma, H. and H. Saito, Evaluation of the three-dimensional configuration of a subsurface artificial fracture by the triaxial shear shadow method, *Geophysics, 56*, 2118-2128, 1991.

Oppenheim, A. V. and R. W. Schafer, *Digital Signal Processing*, 237 pp., Prentice Hall, Englewood Cliffs, New Jersey, 1975.

Pyrak-Nolte, L. J. and N. G. Cook, Elastic interface waves along a fracture, *Geophys, Res. Lett., 14*, 1107-1110, 1987.

Samson, J. C., Matrix and stokes vector representations of detectors for polarized waveforms: theory, with some applications to teleseismic waves, *J. R. astr. Soc., 51*, 583-603, 1977.

K. Nagano and K. Sato, Department of Computer Science and Systems Engineering, Muroran Institute of Technology, Muroran, 050, Japan.
(e-mail: nagano@muroran-it.ac.jp, satoh@csse.muroran-it.ac.jp)

H. Niitsuma, Department of Geoscience and Technology, Graduate School of Tohoku University, Sendai, 980-77, Japan.
(e-mail: niitsuma@ni4.earth.tohoku.ac.jp)